

2017-01-01

# TLS-bridged co-prediction of tree-level multifarious stem structure variables from worldview-2 panchromatic imagery: a case study of the boreal forest

---

Yi Lin, Tian Wei, Bin Yang, Yuri Knyazikhin, Yuhu Zhang, Hisashi Sato, Xing Fang, Xinlian Liang, Lei Yan, Shanlin Sun. 2017. "TLS-bridged co-prediction of tree-level multifarious stem structure variables from worldview-2 panchromatic imagery: a case study of the boreal forest." INTERNATIONAL JOURNAL OF DIGITAL EARTH, Volume 10, Issue 7, pp. 701 - 718 (18).

<https://hdl.handle.net/2144/27433>

*"Downloaded from OpenBU. Boston University's institutional repository."*

# **The spectral invariant approximation within canopy radiative transfer to support the use of the EPIC/DSCOVR oxygen B-band for monitoring vegetation**

Alexander Marshak (NASA/GSFC) and Yuri Knyazikhin (Boston University)

## **Abstract**

EPIC (Earth Polychromatic Imaging Camera) is a 10-channel spectroradiometer onboard DSCOVR (Deep Space Climate Observatory) spacecraft. In addition to the near-infrared (NIR, 780 nm) and the ‘red’ (680 nm) channels, EPIC also has the O<sub>2</sub> A-band (764±0.2 nm) and B-band (687.75±0.2 nm). The EPIC Normalized Difference Vegetation Index (NDVI) is defined as the difference between NIR and ‘red’ channels normalized to their sum. However, the use of the O<sub>2</sub> B-band instead of the ‘red’ channel mitigates the effect of atmosphere on remote sensing of surface reflectance because O<sub>2</sub> reduces contribution from the radiation scattered by the atmosphere. Applying the radiative transfer theory and the spectral invariant approximation to EPIC observations, the paper provides supportive arguments for using the O<sub>2</sub> band instead of the red channel for monitoring vegetation dynamics. Our results suggest that the use of the O<sub>2</sub> B-band enhances the sensitivity of the top-of-atmosphere NDVI to the presence of vegetation.

**Keywords:** EPIC/DSCOVR; O<sub>2</sub> B-band; atmosphere; radiative transfer; vegetation; spectral invariant approximation

## **1. Introduction**

EPIC (Earth Polychromatic Imaging Camera) is a 10-channel spectroradiometer (317 – 780 nm) onboard DSCOVR (Deep Space Climate Observatory) spacecraft. EPIC provides 10 narrow band spectral images of the entire sunlit face of Earth from sunrise to sunset. The DSCOVR spacecraft is located at the Earth-Sun Lagrange-1 (L1) point giving EPIC a unique angular perspective at almost backscattered direction with scattering angle between 168° and 176°. EPIC level 1 data is available from the NASA Langley Atmospheric Science Data Center (ASDC) ([https://eosweb.larc.nasa.gov/project/dscovr/dscovr\\_table](https://eosweb.larc.nasa.gov/project/dscovr/dscovr_table)).

In addition to the ‘red’ (680 nm), ‘green’ (551 nm), ‘blue’ (443 nm), and the NIR (780 nm) channels, EPIC also has two O<sub>2</sub> absorbing channels: the A-band (764±0.2 nm) and B-band (687.75±0.2 nm). The EPIC Normalized Difference Vegetation Index (NDVI) used to monitor the vegetation dynamics is defined as the difference between NIR and ‘red’ channels normalized to their sum (Tucker, 1979). Obviously, at least for dense vegetation, if atmospheric correction is not accurate enough or there are thin clouds in the field of view of EPIC, the NDVI will be biased towards smaller values and the density of vegetation will be underestimated. Can the effect of atmosphere on remote sensing of surface reflectance be mitigated if the O<sub>2</sub> B-band is used instead of the ‘red’ channel?

Consider the top-of-atmosphere (TOA) bidirectional reflection factor (BRF)  $R_\lambda$  expressed as

$$R_\lambda(\Omega, \Omega_0) = \exp\left(-\frac{\tau_\lambda}{|\mu_0|}\right) \rho_\lambda(\Omega, \Omega_0) \exp\left(-\frac{\tau_\lambda}{\mu}\right) + D_\lambda . \quad (1)$$

As usual, here  $\Omega=(\mu, \varphi)$  and  $\Omega_0=(\mu_0, \varphi_0)$  are the directions of reflected and the incident radiation with  $\mu$  and  $\mu_0$  are cosines of viewing and solar zenith angles, and  $\varphi$  and  $\varphi_0$  are viewing and solar azimuthal angles, respectively;  $\tau_\lambda$  is the wavelength dependent optical depth of atmosphere above the surface and  $\rho_\lambda(\Omega, \Omega_0)$  is the surface BRF. The exponential factors describe the attenuation of incoming and reflected solar radiation. Due to the Forbes effect (Ohvri et al., 1999), the total attenuation can be smaller than Eq. (1) predicts. Here this effect is neglected, i.e., it is assumed that the attenuation is described by the optical thickness  $\tau_\lambda$ . Finally,  $D_\lambda$  represents the diffuse radiation due to multiple scattering in atmosphere caused by the incoming and surface reflected radiation as well as surface-atmosphere multiple scattering. At  $\lambda=680$  nm, a typical green leaf absorbs about 95% (Gates et al., 1965) of radiation and thus canopy BRF is low, and the atmospheric contribution to the total TOA BRF,  $R_{680}$ , therefore dominates. Conversely, green leaves absorb less than 10% (Gates et al., 1965) of the incoming radiation at  $\lambda=780$  nm. The surface contribution is consequently increased while the atmospheric contribution does

not change much compared to 680 nm. As a result, the atmospheric contribution to the TOA BRF at 680 nm exceeds that at 780 nm many times.

There are two remarkable features of the EPIC O2 B-band channel images. First, due to oxygen absorption in the earth atmosphere, the diffuse radiation  $D_\lambda$  is substantially reduced, i.e., as the first approximation, we can assume that

$$D_\lambda \approx 0. \quad (2)$$

Second, the BRF of the vegetation reaches its maximum values in the backscattering directions, i.e., when  $\Omega_0 \approx -\Omega$ . This is the so-called hot spot effect: a sharp increase in canopy reflected radiation when scattering direction approaches the backward direction to the sun (e.g., Ross and Marshak, 1989; Kuusk, 1991; Qin et al., 1996). The EPIC sensor therefore sees the brightest portion of the canopy reflected radiation.

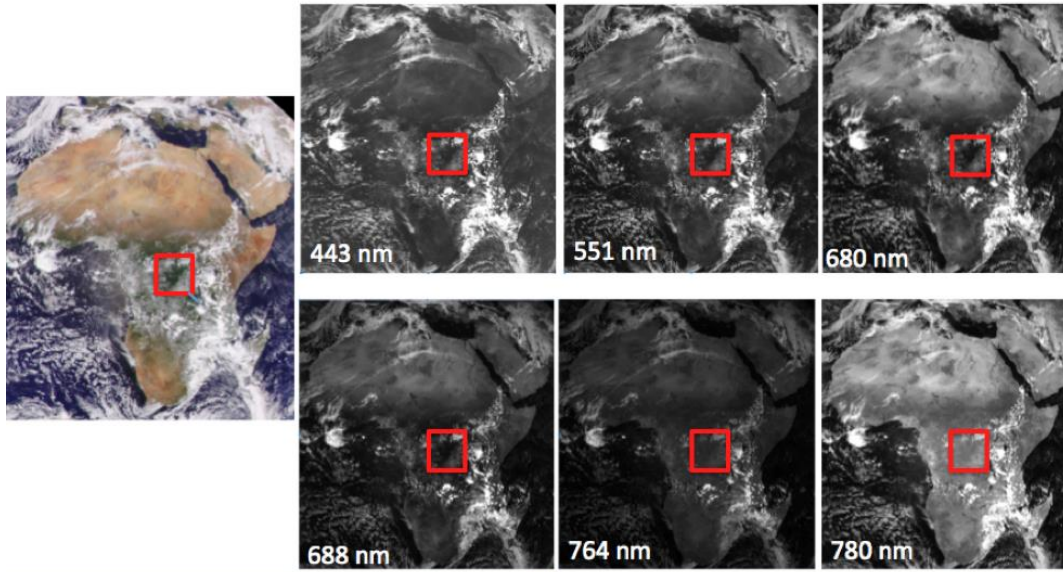


**Figure 1.** EPIC TOA reflectance at six bands measured on March 22, 2016 at 10:52 GMT together with the enhanced and Rayleigh corrected RGB image (see, <http://epic.gsfc.nasa.gov/enhanced>) shown on left panel. The area of interest is highlighted.  $SZA=6.4^\circ \pm 0.5^\circ$ ,  $|\mu_0|=0.994 \pm 0.001$ ;  $VZA=12.7^\circ \pm 0.5^\circ$ ,  $\mu=0.976 \pm 0.002$ ; scattering angle is  $171.5^\circ$ .

Figure 1 shows the enhanced RGB image of Africa and Arabian Peninsula along with the TOA BRF,  $R_\lambda$ , for six EPIC wavelengths acquired on March 22, 2016. The highlighted area of interest here is a mostly cloud-free equatorial dense forest in the middle of the image centered at the Salong National Park (South), Republic of the Congo ( $2.9^\circ \pm 1.0^\circ$  S latitude and  $22.6^\circ \pm 0.5^\circ$  E longitude).

TOA BRF in the near retro-illumination direction is

$$R_\lambda(\Omega, \Omega_0) = \exp\left(-\frac{\tau_\lambda}{|\mu_0|}\right) \rho_\lambda(\Omega, \Omega_0) \exp\left(-\frac{\tau_\lambda}{\mu}\right) + D_\lambda \approx \rho_\lambda(\Omega, \Omega_0) \exp\left(-\frac{2\tau_\lambda}{\mu}\right) + D_\lambda. \quad (3)$$

While the properties of the reflected radiation at the RGB (443, 551, 680 nm) and NIR (780 nm) channels have been well studied for many years, the properties of the reflected radiation from vegetated surface at the O2 absorbing channels are less known. For the dense vegetation at the area of interest in Fig. 1, the simple ratio  $SR = R_{780}/R_{680} \approx 5.6 \pm 0.2$ , while for absorbing channels, because of a stronger absorption at the O2 A-band than at the B-band, this ratio is almost twice smaller, i.e.,  $R_{764}/R_{688} \approx 2.9 \pm 0.1$ . Based on Eqs. (2)-(3),

$$\frac{R_{764}}{R_{688}} \approx \frac{\rho_{764}}{\rho_{688}} \exp\left[-\frac{2(\tau_{764} - \tau_{688})}{\mu}\right], \quad (4a)$$

while

$$\frac{R_{780}}{R_{680}} = \frac{\rho_{780} \exp\left(-\frac{2\tau_{780}}{\mu}\right) + D_{780}}{\rho_{680} \exp\left(-\frac{2\tau_{680}}{\mu}\right) + D_{680}} \quad (4b)$$

The optical depths of the O2 absorbing A- and B-bands were determined using line-by-line calculations of direct transmittance weighted by the EPIC filter functions (see, <http://epic.gsfc.nasa.gov/epic.html>) as  $\tau_{A\text{band}}=0.661$  and  $\tau_{B\text{band}}=0.273$ . Including molecular

scattering ( $\tau_{\text{Rayleigh}764}=0.026$  and  $\tau_{\text{Rayleigh}688}=0.039$ ) but ignoring atmospheric aerosol, we have  $\tau_{764}=0.661+0.026=0.687$  and  $\tau_{688}=0.273+0.039=0.312$ . Finally, we get  $\exp[-2(\tau_{764} - \tau_{688})/\mu] \approx 1/2$ , as observed in Fig. 1. This confirms that while the TOA simple ratio based on the standard red and NIR bands is largely driven by surface properties (biased by scattering atmosphere), the ratio of the O2 B to A-bands is strongly influenced by the O2 absorbing properties.

Note that fluorescence emission by vegetation may also enhance the apparent reflectance of vegetation at the O2 absorption band. However, the maximum signal from fluorescence in the O2 B-band is about 1 mW/m<sup>2</sup>/nm/sr (see Fig. 1 in Joiner et al., 2016) which is well within EPIC calibration uncertainties. Moreover, since it emits at most to a few percent (French, 1960, Gates et al., 1965), the fluorescence has negligible effect on the shape of the leaf reflectance spectrum, e.g., the jump in the red edge. The jump is the key feature of the vegetation BRF that makes the NDVI a reliable indicator of the presence of vegetation. The paper shows that at-sensor 780&688 NDVI is more sensitive to the presence of vegetation compared to its 780&680 NDVI counterpart.

## **2. A brief excursion into the spectral invariant theory in vegetated canopy and its application to EPIC observations**

The spectral surface BRF of dense vegetation such as equatorial forests can be represented as

$$\rho_{\lambda}(\Omega, \Omega_0) = K(\Omega, \Omega_0)W_{\lambda} \quad (5)$$

The coefficient  $K$  is the Directional Area Scattering Factor (DASF), defined as the canopy BRF with non-absorbing Lambertian leaves (Knyazikhin et al., 2013). This wavelength independent variable is determined entirely by canopy geometrical properties such as shape and size of the tree crowns, spatial distribution of trees on the ground and within-crown foliage arrangement. The canopy BRF to  $K$  ratio ( $W_{\lambda} = \rho_{\lambda}/K$ ) is the canopy scattering coefficient; it is an estimate of the fraction of the canopy intercepted radiation

that has been reflected from, or diffusely transmitted through, canopy. The spectral behavior of  $W_\lambda$  is mainly determined by the absorption properties of leaf biochemical constituents and canopy structure. Lewis and Disney (2007) found that the scattering coefficient could be approximated as

$$W_\lambda = \omega_{0\lambda} \frac{1 - p}{1 - p\omega_{0\lambda}}, \quad (6)$$

where the wavelength independent parameter  $p$ , called the recollision probability, depends on the canopy structural organization, and  $\omega_{0\lambda}$  is related to absorption spectrum,  $A_\lambda$ , of leaf biochemical constituents as  $\omega_{0\lambda} = \exp(-A_\lambda)$ . In the spectral range between 500 and 800 nm the leaf chlorophyll and dry matter mainly absorb radiation. The former varies with wavelength whereas the latter is flat, i.e.,  $A_\lambda = \alpha k_{ch,\lambda} + \beta$ . Here  $k_{ch,\lambda}$  is the chlorophyll absorption spectrum,  $\alpha$  is its concentration and  $\beta$  represents the total absorption coefficient of dry matter. The spectrum of  $\omega_{0\lambda}$  can be parameterized as

$$\omega_{0\lambda} = \exp(-A_\lambda) = \exp[-(\alpha k_{ch,\lambda} + \beta)]. \quad (7)$$

Thus the spectral variation of the scattering coefficient  $W_\lambda$  is fully determined by the chlorophyll absorption spectrum. Various spectral indices defined in the 500-800 nm spectral range therefore are determined by the spectral properties of the chlorophyll absorption.

Note that multiplying Eq. (6) by  $K$  and using Eq. (5) we can see (e.g., Huang et al., 2007; Lewis and Disney, 2007, Knyazikhin et al., 2011; Marshak et al., 2011) that it is identical to

$$\frac{\rho_\lambda}{\omega_{0\lambda}} = p\rho_\lambda + K(1 - p), \quad (8)$$

i.e., for dense vegetation the ratio  $\rho_\lambda/\omega_{0\lambda}$  is linearly related to  $\rho_\lambda$  for wavelengths between 500 and 800 nm. The slope,  $p$ , and the intercept,

$$b(\Omega, \Omega_0) = K(\Omega, \Omega_0)(1 - p) \quad (9)$$

of this linear relationship depend on both  $\alpha$  and  $\beta$ . The ratio,  $K(\Omega, \Omega_0) = b(\Omega, \Omega_0)/(1 - p)$ , however, becomes independent on the concentrations  $\alpha$  and  $\beta$  and results in the directional area scattering factor (Knyazikhin et al., 2013). This property underlies a simple algorithm to decompose canopy spectral BRF,  $\rho_\lambda$ , into structural,  $K$ , and radiometric wavelength-dependent component  $W_\lambda$ .

Next multiplying both parts of Eq. (8) by  $\exp(-2\tau_\lambda/\mu)$  and using Eq. (3), we get

$$\frac{R_\lambda(\Omega, \Omega_0)}{\omega_{0\lambda}} = pR_\lambda(\Omega, \Omega_0) + b(\Omega, \Omega_0) \exp\left(-\frac{2\tau_\lambda}{\mu}\right) + D_{A\lambda} \quad , \quad (10)$$

where  $D_{A\lambda} = D_\lambda(1 - p)W_\lambda^{-1}$ . We applied Eq. (10) directly to known TOA BRF  $R_\lambda$  and  $R_\lambda/\omega_{0\lambda}$  instead of unknown surface BRF  $\rho_\lambda$  and  $\rho_\lambda/\omega_{0\lambda}$  at two wavelengths  $\lambda$  [NIR (780 nm) and green (551 nm)] to, first, calculate slope and intercept of a line connecting two points,  $(R_\lambda, R_\lambda/\omega_{0\lambda})$ ,  $\lambda = 551$  nm, 780 nm, and, second, to obtain an estimate,  $\tilde{K}$ , of the coefficient  $K$ . Numerical analyses suggest that  $\tilde{K}$  is weakly sensitive to the variability of the atmospheric optical depth  $\tau_\lambda$  (e.g.,  $\tau_{551}=0.1$  leads to a less than 2% increase in  $\tilde{K}$ ) if  $D_{A\lambda} \approx 0$ . In this case Eq. (10) provides an estimate of spectrally independent parameter  $K$  which is proportional to its true value and independent on chlorophyll concentration  $\alpha$  and absorption coefficient  $\beta$ . An increase of  $D_{A\lambda}$  introduces dependency on  $\alpha$  and  $\beta$  into  $\tilde{K}$ , making it more uncertain.



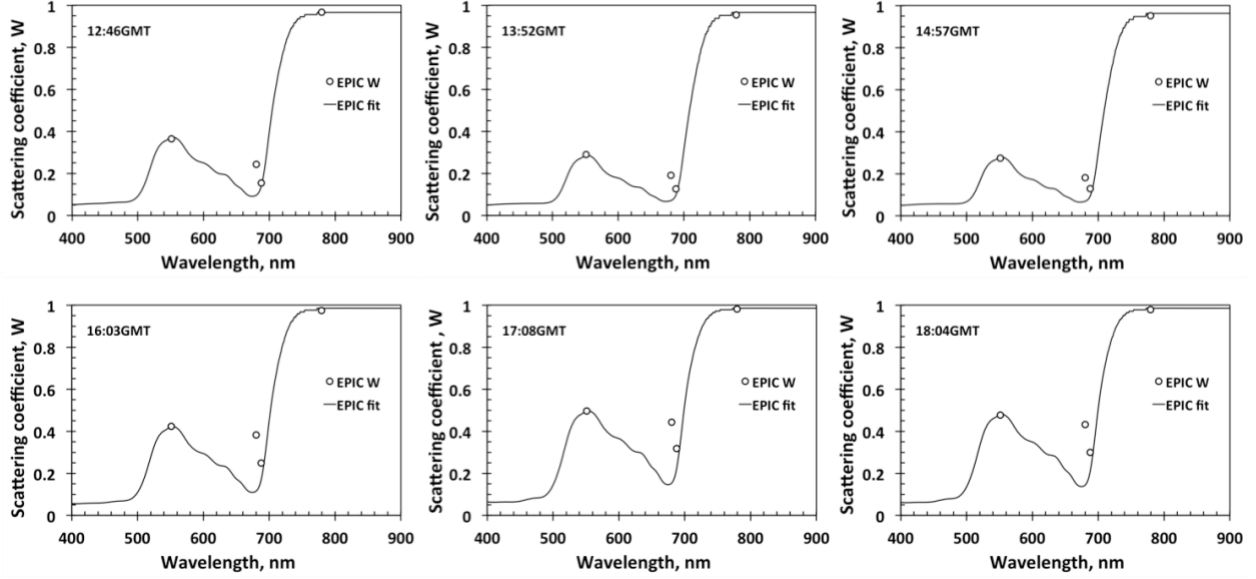


**Figure 2.** Spectrally variable scattering coefficient  $W_\lambda$  obtained from EPIC observations taken on Sep. 23, 2015 at 6 different GMT times (GMT = local time + 4 h) over a 20 km area around point (4.4S, 68.1W) in Amazonian rainforests. The scattering angle is  $173.4^\circ$ . Four EPIC bands ( $\lambda = 551, 680, 688$  and  $780$  nm) are shown with open circles while the line is  $\tilde{W}_\lambda$  fitted with Eq. (6). Note that cloudiness (and  $W_\lambda$ ) increases with GMT time (see, <http://epic.gsfc.nasa.gov>).

An approximation,  $\tilde{W}_\lambda$ , to the scattering coefficient  $W_\lambda$  at  $\lambda = 551, 688$  and  $780$  nm can be obtained by normalizing the TOA BRF,  $R_\lambda$ , with  $\tilde{K}$ . Using Eq. (3) it can be shown that  $\tilde{W}_\lambda$  is linearly related to  $W_\lambda$  as

$$\tilde{W}_\lambda = \exp(-2\tau_\lambda/\mu) \frac{K}{\tilde{K}} W_\lambda + \frac{D_\lambda}{\tilde{K}}. \quad (11)$$

Figure 2 illustrates that the linear transformation preserves the shape of the spectral scattering coefficient  $W_\lambda$  over dense vegetation although its magnitude is overestimated: the term  $D_\lambda/\tilde{K}$  that describes the contribution from the radiation scattered by the atmosphere causes an upward shift of the scattering coefficient. The line shows the scattering coefficient fitted with Eqs. (6) and (7). One can see that Eq. (6) always fits the scattering coefficient at  $\lambda = 551, 688$  and  $780$  nm independently of (transparent) atmospheric conditions (aerosols or thin clouds) while its value at  $\lambda = 680$  nm fails to be

fitted. At this wavelength the second term in the right hand side of Eq. (11) dominates making  $\tilde{W}_{680} > \tilde{W}_{688}$  while for the ‘true’ values of the scattering coefficient,  $W_{680} < W_{688}$ . Finally we note that though  $D_{764} \approx 0$ , much stronger atmospheric absorption at the O2 A-band causes a significant distortion of the spectral shape of the scattering coefficient near 764 nm.

Since atmospherically corrected EPIC surface BRF is not yet available, in Fig. 3 we used the atmospherically corrected Multi-angle Imaging SpectroRadiometer (MISR) surface BRF,  $\rho_\lambda$ , over the same forested area and the same sun-sensor geometry as in Fig. 2 (13:52GMT) to obtain an accurate estimate of the parameter  $K$  and the scattering coefficient  $W_\lambda$ . Values of the MISR scattering coefficient at  $\lambda = 558, 672$  and  $860$  nm are shown as circles. The diamonds depict the EPIC scattering coefficient obtained by normalizing EPIC TOA BRF,  $R_\lambda$ , by the wavelength independent parameter  $K$  obtained from MISR. Its values are overestimated at  $\lambda = 551, 680$  and  $688$ , but accurate at  $780$  nm, as expected. Similar to Fig. 2, the dotted line approximates  $\tilde{W}_\lambda$  at  $551$  and  $688$ , but not at  $680$  nm. Note that the normalization of TOA EPIC BRF by the EPIC parameter  $\tilde{K}$  increases  $\tilde{W}_\lambda$  (cf. Fig. 2, panel 13:52GMT). This, however, does not violate the relationship between the chlorophyll absorption spectrum and the scattering coefficient at  $551, 688$  and  $780$  nm.

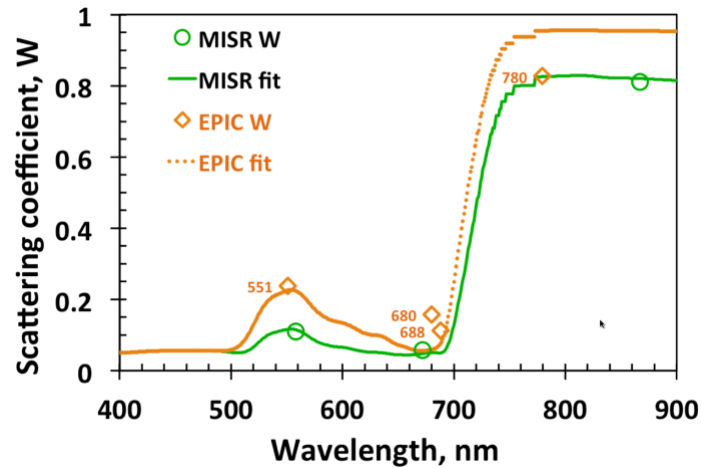


**Figure 3.** Canopy scattering coefficient from EPIC at 551, 680, 688 and 780 nm (diamonds) and MISR at 558, 672, and 867 nm (circles). Shown are  $W_\lambda$  for MISR and  $W_\lambda \exp(-2\tau_\lambda) + D_\lambda$  for EPIC at 13:52GMT.

To summarize Figs. 2 and 3, the estimate  $\tilde{W}_\lambda$  of the scattering coefficient at  $\lambda = 551, 688$  and  $780$  nm (but not at  $\lambda = 680$  nm) can be well approximated by the chlorophyll absorption spectrum. Because chlorophyll absorption is the only absorbing leaf constituent, radiation reflected by dense vegetation and passed through the atmosphere at these wavelengths is very sensitive to the presence of vegetation: indeed, forests can be seen even through thin clouds.

### 3. Chlorophyll absorption spectrum and NDVI

The above examples indicate that impact of the atmosphere on the TOA BRF,  $R_\lambda$ , minimally impacts the relationship between the scattering coefficient and chlorophyll absorption spectrum at  $\lambda = 688$  and  $780$  nm. The Normalized Difference Vegetation Index (NDVI) is the key indicator of the presence of the chlorophyll in remote sensing. The EPIC NDVI is defined as

$$NDVI = \frac{R_{NIR} - R_{red}}{R_{NIR} + R_{red}} = \frac{SR - 1}{SR + 1}. \quad (12)$$

Here  $SR = R_{NIR}/R_{red}$  is the simple ratio between the TOA BRF at the NIR and red channels. If the atmospheric impact is small, the NDVI is mainly determined by the chlorophyll concentration,  $\alpha$ , and canopy structural organization. We will show below that impact of the atmosphere is smaller if the EPIC O2 B-band channel (688 nm) is used instead of the EPIC red channel (680 nm). We start with the simple ratio; it can be approximated as

$$SR = \frac{R_{NIR}}{R_{red}} = \frac{\rho_{NIR} \exp\left(-\frac{2\tau_{NIR}}{\mu}\right) + D_{NIR}}{\rho_{red} \exp\left(-\frac{2\tau_{red}}{\mu}\right) + D_{red}}. \quad (13a)$$

$$\approx \frac{\rho_{NIR}}{\rho_{red}} = \frac{K W_{NIR}}{K W_{red}} = \frac{W_{NIR}}{W_{red}} \quad (13b)$$

$$\approx \frac{\omega_{0,NIR}}{\omega_{0,red}} = \exp[-\alpha(k_{ChNIR} - k_{Chred})] \quad (13c)$$

$$\approx \exp(\alpha k_{Chred}) \quad (13d)$$

The ratio between  $\ln(SR)$  and the known difference  $k_{Chred}$  is determined by the chlorophyll concentration,  $\alpha$ . Note that  $k_{ChNIR} \approx 0$ , i.e., the NIR absorption coefficient  $A_{NIR} \approx \alpha k_{ChNIR} + \beta = \beta$ .

The approximation (13c) to (13d) is based on the fact that  $k_{ChNIR} \approx 0$ . The approximation between (13b) and (13c) is based on Eq. (6) if one neglects the ratio  $(1-p\omega_{0red})/(1-p\omega_{0NIR})$ . The approximation between (13a) and (13b) is based on two assumptions. First, it ignores the attenuation by the Earth atmosphere in both channels,  $[\exp(-2\tau_\lambda/\mu)]$ . Second, it ignores the contribution of multiple scattering (diffuse radiation:  $D_{NIR}$  and  $D_{red}$ ). Note that the second assumption is much better met with the 688-nm channel than with the 680-nm one.

Regarding neglecting the ratio  $(1-p\omega_{0red})/(1-p\omega_{0NIR})$  we note that the right hand side of Eq. (6) can be approximated as  $\omega_{0\lambda}(1-p)/(1-p\omega_{0\lambda}) \approx \omega_{0\lambda}^m$ , where the power  $m$  depends on  $p$  and chlorophyll concentration,  $\alpha$ . This approximation is very accurate for weakly absorbing wavelengths (Yang et al., 2016). Lewis and Disney (2007) used this approximation for all wavelengths and found that a large portion of variation in  $W_\lambda$  is due to variation in  $m$ . It follows from here that  $\ln(W_{NIR}/W_\lambda)$  is proportional to the chlorophyll absorption spectrum  $k_{Ch,\lambda}$  in the range between 500 and about 800 nm, which is a strong indication of the presence of green leaves.

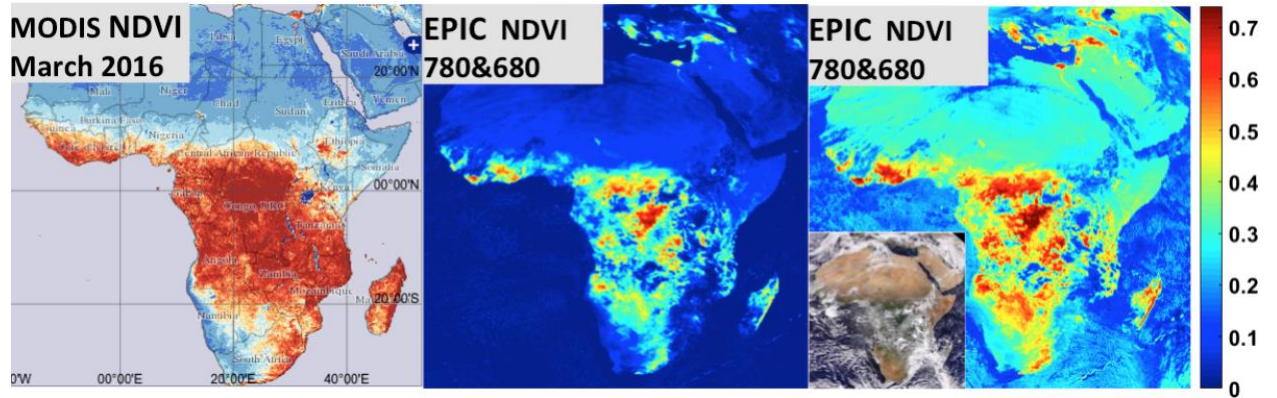


**Figure 4.** The left panel shows MODIS/Terra surface NDVI composited over March, 2016 (<https://giovanni.gsfc.nasa.gov/giovanni/>). The middle and the right panels are EPIC NDVIs for March 22,

2016 (10:52 GMT) calculated with the red and O2 B-band channels, respectively. The insert in the right panel is the RGB plot from Fig. 1 (left panel). The use of the O2 B-band enhances the sensitivity of the TOA NDVI to the presence of vegetation.

To illustrate the above points, Fig. 4 shows two EPIC NDVIs: one with the red channel and one with the O2 B-band one. We see that the second NDVI (right panel) provides a much better signature of the dense vegetation in the cloud-free regions of the Salong National Park in the Republic of the Congo at the middle of the image (2.9S, 22.6E) than the first NDVI (middle panel). Interestingly, the O2 B-band NDVI indicates the dense vegetated areas at the east cost of Madagascar (as it should be, see <https://www.google.com/maps/@-19.7458922,42.9011667,3283813m/data=!3m1!1e3>) that is partly covered by clouds in the RGB image at the left panel (it could also be affected by an imperfect geolocation between the two images). In addition, note that the vegetated areas in West Africa (e.g. Ghana, Liberia, Sierra-Leone) are clearly observed with the new NDVI at the right panel. This is because the 780&688 NDVI better corresponds to the chlorophyll absorption spectrum compared to its 780&680 counterpart. In other words, the use of O2 B-band enhances the sensitivity of the TOA NDVI to the presence of vegetation.

To conclude, the 780&688 NDVI is closer to the atmospherically corrected NDVI than its standard 780&680 counterpart. This is a consequence that the atmosphere minimally impacts the relationship between the scattering coefficient  $W_\lambda$  and the chlorophyll spectrum  $A_\lambda$ ; the later is the key indicator of green leaves. Note that the relationship (6) for  $W_\lambda$  takes place if and only if the chlorophyll is present.

Finally, Fig. 5 shows the enhanced RGB image taken on Sep-23-2015 at 13:52 GMT and corresponding false color image (688-551-680) of the scattering coefficient  $W_\lambda$ . This image suggests that the relationships  $W_{551} > W_{680} > W_{688}$  for vegetated surfaces shown in Fig. 2 and discussed in Sect. 3 holds globally, making the TOA 780&688 NDVI more sensitive to the presence of vegetation even in case of aerosol and thin-cloud contamination.

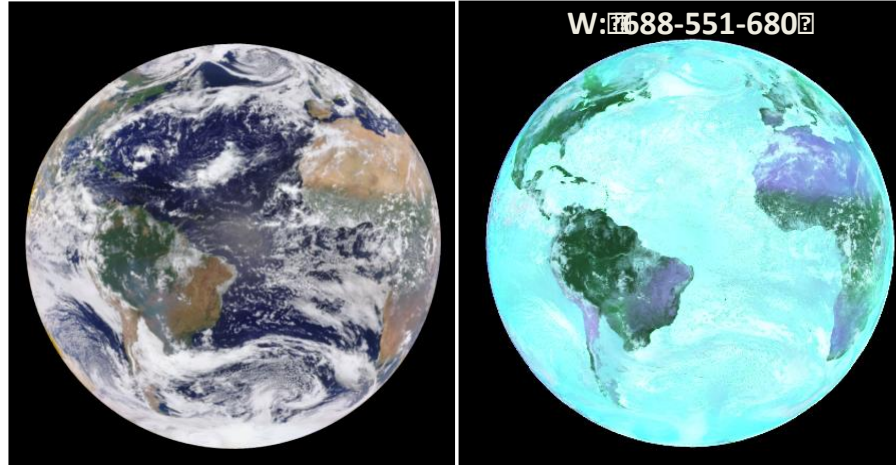


**Figure 5.** Left panel shows an enhanced RGB image of the sunlit face of the Earth (<http://epic.gsfc.nasa.gov/enhanced>) taken on Sep-23-2015 at 13:52GMT. Right panel is the false color image (688-551-680) of the scattering coefficient  $W_\lambda$ ; it illustrates a strong sensitivity to the presence of green leaves.

#### 4. Summary

The EPIC onboard DSCOVR spacecraft is located at the Earth-Sun L1 point ( $\sim 1.5$  mln km from Earth towards Sun); it provides 10 narrow band spectral images of the entire sunlit face of Earth from sunrise to sunset in near backscattering directions with the scattering angle between  $168^\circ$  and  $176^\circ$ . The EPIC Normalized Difference Vegetation Index (NDVI) defined as the ratio between the difference and the sum of the NIR (780 nm) and the red (680 nm) channels is used to monitor vegetation dynamics. An accurate estimate of vegetation density requires an accurate atmospheric correction. This papers shows that if the EPIC O2 B-band (688 nm) is used instead of the red band, the effect of atmosphere (the diffuse radiation) on remote sensing of surface reflectance will be reduced and the residual uncertainties in atmospheric correction can be better tolerated. This is due to two factors: (i) vegetated surface is yet sufficiently dark at 688 nm and (ii) the O2 absorbing atmosphere substantially reduces multiple scattering.

To support this statement, the spectral invariant approximation of the BRF of vegetated surface (Stenberg et al., 2016) was used. It was shown that the retrieval of spectrally invariant coefficient  $K$  (known as the Directional Area Scattering Factor (DASF), Knyazikhin

et al., 2013), a purely canopy structural variable, is only weakly sensitive to the uncertainties in the spectral properties of the atmospheric optical depth  $\tau_\lambda$  above the canopy. The coefficient  $K$  is estimated as the ratio between the intercept and 1-slope as stated in Eqs. (9) and (10). The spectral scattering coefficient  $W_\lambda$ , from the other hand, is fully determined by the chlorophyll absorption spectrum and can be estimated from the TOA BRF and the approximated coefficient  $K$  using Eq. (5). We demonstrated (Figs. 2 and 3) that the approximated values of  $W_\lambda$  at  $\lambda = 551, 688$  and  $780$  nm fit the spectral shape of the ‘true’ scattering coefficient over dense vegetation (see Eq. (6)) for all atmospheric conditions observed in Figs. 2 and 3. However, in contrast to  $W_{688}$ , the values of  $W_{680}$  obtained from Eq. (5) are always above the spectral curve determined by chlorophyll spectrum, exceeding  $W_{688}$  by 30-35%.

Figures 4 illustrates two NDVIs with 780&680 (middle panels) and 780&688 (right panels) over Africa where we can clearly see that the 780&688 NDVI better identifies patterns of dense vegetation compared to the 780&680 NDVI. This is because without an accurate atmospheric correction the 780&688 NDVI is more sensitive to the presence of the chlorophyll than the standard 780&680 one. Equation (13) uses the simple ratio between the two TOA BRFs at NIR and red to formally support this conclusion. Finally, Fig. 5 complements Fig. 2 and suggests that the above approach can be extended to the global scale.

**Acknowledgment.** This research was supported by the NASA DSCOVR project supervised by Richard Eckman as the technical officer. We thank Bin Yang for processing MISR BRF. We also thank Karin Blank, Jay Herman, Adam Szabo and Yuekui Yang for insightful discussions and help with EPIC data. The EPIC ([https://eosweb.larc.nasa.gov/project/dscovr/dscovr\\_table](https://eosweb.larc.nasa.gov/project/dscovr/dscovr_table)) and MISR ([https://eosweb.larc.nasa.gov/project/misr/misr\\_table](https://eosweb.larc.nasa.gov/project/misr/misr_table)) data were obtained from the NASA Langley Research Center Atmospheric Science Data Center (ASDC).

## References

French, C.S. (1960). The chlorophylls in vivo and in vitro. In A. Pirson (Ed.), *Die CO<sub>2</sub>-Assimilation / The Assimilation of Carbon Dioxide: In 2 Teilen / 2 Parts* (pp. 252-297).



352 Berlin, Heidelberg: Springer Berlin Heidelberg.  
 353 Gates, D.M., Keegan, H.J., Schleter, J.C., & Weidner, V.R. (1965). Spectral properties of plants.  
 354 *Applied Optics*, 4, 11-20.  
 355 Huang, D., Y. Knyazikhin, R. E. Dickinson, M. Rautiainen, P. Stenberg, M. Disney, et al., 2007.  
 356 Canopy spectral invariants for remote sensing and model applications. *Remote Sens.*  
 357 *Environ.*, 106, 106–122.  
 358 Joiner, J. Y. Yoshida, L. Guanter, and E. M. Middleton, 2016. New methods for the retrieval of  
 359 chlorophyll red fluorescence from hyperspectral satellite instruments: simulations and  
 360 application to GOME-2 and SCIAMACHY, *Atmos. Meas. Tech.*, 9, 3939-3967.  
 361 Knyazikhin, Y., M.A., Schull, X., Liang, R.B, Myneni, and A. Samanta, 2011. Canopy spectral  
 362 invariants. Part 1: A new concept in remote sensing. *J. Quant. Spectrosc. Radiat.*  
 363 *Transfer*, 112, 727–735.  
 364 Knyazikhin, Y., M. A. Schull, P. Stenberg, M. Möttus, M. Rautiainen, Y. Yang, et al., 2013.  
 365 Hyperspectral remote sensing of foliar nitrogen content. *Proc. Nat. Acad. Sci.*, 110,  
 366 E185-E192.  
 367 Kuusk, 1991. The hot spot effect in plant canopy reflectance. In R.B. Myneni, & J. Ross  
 368 (Eds.), *Photon-vegetation interactions: applications in plant physiology and optical*  
 369 *remote sensing* (pp. 139-159). Berlin Heidelberg: Springer-Verlag.  
 370 Lewis, P. and M. Disney, 2007. Spectral invariants and scattering across multiple scales  
 371 from within-leaf to canopy. *Remote Sens. Environ.*, 109:196–206.  
 372 Marshak, A., Y. Knyazikhin, J.C. Chiu, and W.J. Wiscombe, 2011. Spectrally-invariant  
 373 approximation within atmospheric radiative transfer. *J. Atmos. Sci.*, 68, 12, 3094-3111.  
 374 Ohvri, H., O. Okulov, H. Teral, and K. Teral, 1999. The atmospheric integral transparency  
 375 coefficient and the Forbes effect. *Solar Energy*, 66, 4, 305-317.  
 376 Qin, W., N.S. Goel, and B. Wang, 1996. The hotspot effect in heterogeneous vegetation  
 377 canopies and performances of various hotspot models. *Remote Sens. Reviews*, 14, 283-  
 378 332.



379 Ross, J. K. and A. L. Marshak, 1989. The influence of leaf orientation and the specular  
 380 component of leaf reflectance on the canopy bidirectional reflectance. *Remote Sens.*  
 381 *Environ.*, 27, 251-260.  
 382 Sternberg, P., M. Möttus, and M. Rautiainen, 2016. Photon recollision probability in  
 383 modelling the radiation regime of canopies — A review. *Remote Sens. Environ.*, 183, 98-  
 384 108.  
 385 Tucker, C. J., 1979. Red and photographic infrared linear combination for monitoring  
 386 vegetation, *Remote Sens. Environ.*, 8, 127-150.  
 387 Yang, B., Y. Knyazikhin, Y. Lin, K. Yan, C. Chen, T. Park, et al., 2016. Analyses of impact of  
 388 needle surface properties on estimation of needle absorption spectrum: Case study  
 389 with coniferous needle and shoot samples. *Remote Sens.* 8, 563;  
 390 doi:10.3390/rs8070563.